

## Back-illuminated separate absorption and multiplication GaN avalanche photodiodes

J. L. Pau,<sup>1</sup> C. Bayram,<sup>1</sup> R. McClintock,<sup>1</sup> M. Razeghi,<sup>1,a)</sup> and D. Silversmith<sup>2</sup>

<sup>1</sup>Center for Quantum Devices, Department of Electrical Engineering and Computer Science, Northwestern University, Evanston, Illinois 60208, USA

<sup>2</sup>Air Force Office of Scientific Research, Arlington, Virginia 22203, USA

(Received 9 December 2007; accepted 22 February 2008; published online 13 March 2008)

The performance of back-illuminated avalanche photodiodes with separate absorption and multiplication regions is presented. Devices with an active area of  $225 \mu\text{m}^2$  show a maximum multiplication gain of 41 200. The calculation of the noise equivalent power yields a minimum value of  $3.3 \times 10^{-14} \text{ W Hz}^{-1/2}$  at a gain of 3000, increasing to  $2.0 \times 10^{-13} \text{ W Hz}^{-1/2}$  at a gain of 41 200. The broadening of the response edge has been analyzed as a function of bias. © 2008 American Institute of Physics. [DOI: 10.1063/1.2897039]

The investigation of photocurrent gain in (Al)GaN devices is motivated by the need for high sensitivity ultraviolet (UV) detectors in many civilian and military applications. Impact ionization in avalanche photodiodes (APDs) is one of the most effective gain mechanisms, capable of delivering gain factors higher than  $10^3$  in linear mode operation<sup>1,2</sup> and higher than  $10^7$  in the Geiger mode.<sup>3</sup> Ionization coefficients have been demonstrated to be higher for holes than for electrons, which makes back-illuminated GaN *p-i-n* APDs well suited to providing high gains and low noise.<sup>4</sup> Moreover, high gain uniformity and breakdown voltage reproducibility have already been demonstrated in back-illuminated GaN APDs, enabling the fabrication of multipixel arrays.<sup>5</sup> Integration with readout integrated circuits also becomes easier in back-illuminated designs.

Back-illuminated GaN APDs have shown single-photon detection capabilities;<sup>6</sup> however, their performance in linear mode is still limited by the maximum gain achievable and the noise characteristics. The use of separate absorption and multiplication (SAM) regions in APDs is a common approach to reduce multiplication noise and enhance gain through impact-ionization engineering.<sup>7-10</sup> In this work, we present the fabrication and characterization of GaN APDs with a SAM design allowing for nearly pure injection of holes into the multiplication region, potentially offering lower noise performance and benefiting from the higher ionization coefficient for holes.

Samples were grown by metal-organic chemical-vapor deposition on transparent AlN templates on double side polished *c*-plane sapphire substrates. They consisted of *p-i-n-i-n* GaN structures with hole and electron concentrations of  $(1-3) \times 10^{18}$  and  $(1-2) \times 10^{18} \text{ cm}^{-3}$  for the *p*-type GaN:Mg and *n*-type GaN:Si layers, respectively; the *i* regions consisted of undoped GaN with a residual carrier concentration of  $(1-2) \times 10^{16} \text{ cm}^{-3}$ . The full structure and the electric field profile calculated from a one-dimensional finite element model are shown in Fig. 1. At low voltages, the electric field is mainly localized in the topmost *i*-GaN layer (multiplication region). The increase of the reverse bias enhances the electric field in this layer and broadens the depletion region toward the *p*-GaN and across the *n*-GaN layer toward the

other *i*-GaN layer. This intrinsic layer becomes fully depleted at the reach-through voltage ( $V_{\text{rt}}=40 \text{ V}$ ).

Absorption measurements were performed in reference samples, yielding an absorption coefficient of about  $1 \times 10^5 \text{ cm}^{-1}$  at the GaN bandgap energy. From this value, we calculated the percentage of the light absorbed in the bottom *n*-GaN and *i*-GaN layers; those combined layers account for 99% of the absorption and hence are considered to form the absorption region of the device. However, the absorption properties change for photon energies above or below the bandgap: as the photon energy increases above the bandgap, the light becomes mainly absorbed in the bottom *n*-GaN, closer to the AlN interface; contrarily, as the energy decreases below the bandgap, the light becomes mainly absorbed in the upper layers. In particular, the Franz-Keldysh effect may raise the absorption coefficient in the multiplication region at longer wavelengths. The impact of these effects on the spectral response of the device will be discussed later.

Several arrays of  $225 \mu\text{m}^2$  mesa structures were defined via photolithography, dry etching, metal evaporation, and SiO<sub>2</sub> passivation; details of the device fabrication can be found elsewhere.<sup>5</sup> Electro-optic characterization of the devices was performed under back illumination through an UV optical fiber using a 150 W Xe arc lamp. For the spectral response measurements, the lamp was coupled to a

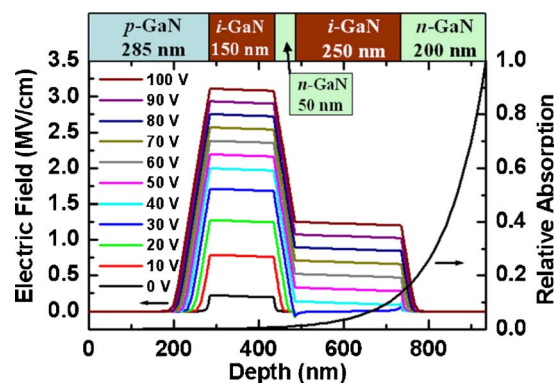


FIG. 1. (Color online) Left axis: electric field profile calculated as a function of reverse bias in the SAM APDs. Right axis: relative absorption for an absorption coefficient of  $1 \times 10^5 \text{ cm}^{-1}$ . The basic structure of the device is depicted at the top.

<sup>a)</sup>Electronic mail: razeghi@eecs.northwestern.edu.

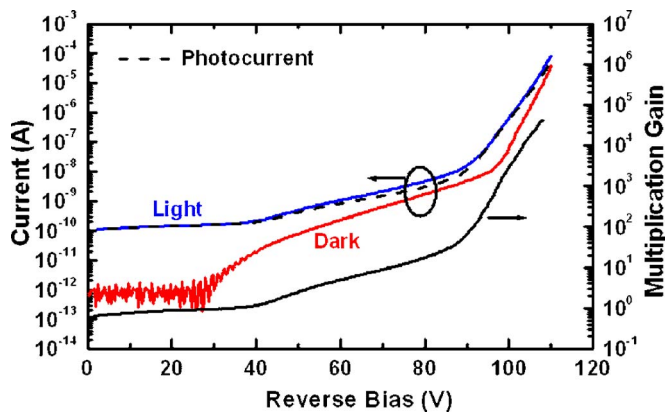


FIG. 2. (Color online) Left axis: dark and light (360 nm) currents measured in the SAM APDs; the dashed line represents the calculated photocurrent. Right axis: calculated gain.

monochromator/chopper setup and the device was connected to a lock-in amplifier.

The current-voltage ( $I$ - $V$ ) characteristics under reverse bias were measured in darkness and under illumination using the Xe lamp filtered at 360 nm (Fig. 2). The optical power on the diode was 4.1 nW. The light and dark  $I$ - $V$  curves were measured alternatively three times in a row to ensure consistent device operation. In darkness, the current remains below the measurement limit up to 30 V. Beyond that voltage, dark current increases monotonously until reaching the breakdown voltage at 96 V, at which point the device exhibits a dark current of 10 nA. At this voltage, the electric field profile predicts an average value of about 3 MV/cm in the multiplication region, in fairly good agreement with the value of the critical electric field in GaN.<sup>4</sup> A sharp increase of the dark current is observed above breakdown reaching 81  $\mu$ A at 111 V.

Under 360 nm illumination, the current remains fairly flat between zero and  $V_{rt}$  and then begins to increase with larger reverse bias. To calculate the multiplication gain, we normalized the photocurrent, i.e. difference between light and dark currents, by its nearly constant value at low voltages. Figure 2 shows that the gain increases gradually from  $V_{rt}$ . Near the breakdown voltage, the avalanche multiplication raises the gain up to a maximum value of 41 200 at 108 V.

The spectral response was measured under back illumination as a function of reverse bias [Fig. 3(a)]. At low voltages, the devices present a sharp response at around 364 nm, corresponding to the absorption edge of GaN. The response at shorter wavelengths remains below the background noise of the setup. Those photons are absorbed closer to the AlN interface, and at low voltages, the depletion region remains far from the AlN interface. At  $V_{rt}$ , the depletion region is fully extended, and a peak responsivity of 102.5 mA/W is achieved at 364 nm, corresponding to an external quantum efficiency of greater than 35%. In addition, the optical response at shorter wavelengths becomes evident in the spectrum, increasing for larger bias voltages with the same gain as the peak response.

In order to investigate the response below the bandgap, the wavelength of the responsivity peak and the 20 dB fall-off point were tracked as a function of reverse bias [Fig. 3(b)]. The peak responsivity wavelength does not vary significantly; however, the 20 dB fall-off point clearly redshifts

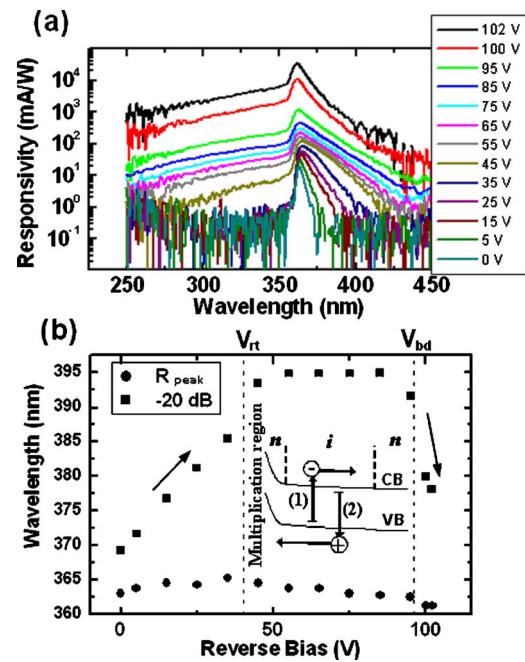


FIG. 3. (Color online) (a) Spectral response measured in the SAM APDs as a function of reverse bias. (b) Wavelength of the responsivity peak ( $R_{peak}$ ) and 20 dB fall-off wavelength ( $-20$  dB) as a function of reverse bias. The arrows indicate the redshift of the response cutoff at low voltages and the blueshift induced by the multiplication process near breakdown. The inset shows the band tailing absorption processes that may account for this behavior.

at low voltages due to the increasing response below the bandgap. This response has been previously attributed to the Franz-Keldysh effect in the multiplication region, which accounts for an increasing absorption coefficient under high electric fields.<sup>11</sup> Contrary to what is expected from this theory, the response stops shifting at voltages higher than  $V_{rt}$ , despite the further monotonous increase of the electric field strength. Moreover, the 20 dB fall-off point starts to blueshift when the bias voltage approaches the breakdown voltage as a result of a lower relative response at longer wavelengths.

The saturation of the redshift at  $V_{rt}$  suggests that the responsible absorption process at longer wavelengths may involve other layers and not only the multiplication region. The light absorption through band tail states can also play an important role, especially as the depletion region width becomes larger. Small absorption coefficients can result in a significant amount of photogenerated carriers in the wide depletion region, contributing to the response below the bandgap. It can make the response shift toward longer wavelengths as the depletion region broadens. However, when the depletion region broadening becomes limited by the pinch off with the bottom  $n$ -GaN layer at  $V_{rt}$ , the spectrum stops shifting.

The inset of Fig. 3(b) shows two possible mechanisms that can account for the anomalous absorption in the intrinsic layer through conduction and valence band tail states. The first mechanism (1) yields an electron that is swept out of the depletion region with a minimal capability of producing ionization events because it does not ever reach the multiplication region. The second mechanism (2) yields a hole that is injected in the multiplication region, potentially undergoing ionization. In the avalanche regime, the gain for longer wavelengths can be handicapped by the ineffective first

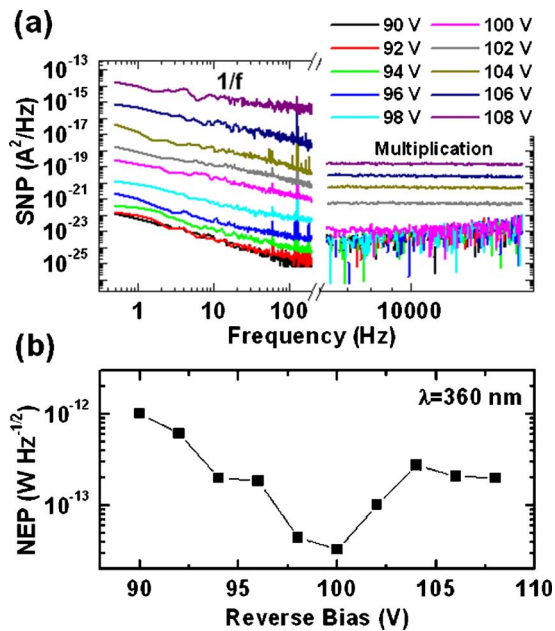


FIG. 4. (Color online) (a) Spectral noise power obtained near breakdown. The broken  $x$  axis separates the low frequency range, in which the  $1/f$  contribution dominates, from the midfrequency range, dominated by the multiplication noise. (b) Calculated NEP vs reverse bias voltage.

mechanism, which may explain the blueshift of the 20 dB fall-off point observed above breakdown.

Noise measurements were performed on these devices in darkness around the breakdown voltage (90–108 V). The signal from the detector was amplified with a low noise transimpedance amplifier ( $10^6$ – $10^7$  V/A) and then analyzed using a fast Fourier transform spectrum analyzer with a 100 kHz bandwidth. As previously published, the noise characteristic of these devices is dominated by the  $1/f$  and multiplication noise contributions at low and medium frequencies, respectively.<sup>4</sup> A 195 Hz span was used to measure the  $1/f$  noise at low frequencies. To determine the multiplication noise, the measurements were also performed in the medium frequency range with a 12.5 kHz span. At low frequencies, the  $1/f$  noise increases monotonously as the reverse bias goes over the breakdown voltage. At intermediate frequencies, the multiplication noise starts to be evident over the noise floor only above the breakdown voltage. At the same gain level, the contribution of the multiplication noise is con-

siderably lower than the multiplication noise observed in regular back-illuminated  $p$ - $i$ - $n$  GaN diodes.

Spectral power density ( $S_n$ ) for  $1/f$  noise was fitted by using  $S_n = s_0 I_d^2 / f^\gamma$ , where  $s_0$  and  $\gamma$  are fitting parameters and  $I_d$  is the dark current. Its associated noise current was calculated and added to the multiplication noise current in order to obtain the noise equivalent power (NEP). The result is depicted in Fig. 4(b) as a function of reverse bias. The NEP has a minimum value of  $3.3 \times 10^{-14}$   $\text{W Hz}^{-1/2}$  at 100 V, which corresponds to a gain of about 3000. At higher and lower voltages, the NEP value increases. In particular, a NEP of  $2.0 \times 10^{-13}$   $\text{W Hz}^{-1/2}$  is obtained at the maximum gain of 41 200.

In conclusion, the performance of back-illuminated GaN APDs with SAM regions has been analyzed. Higher gain and lower noise than in regular  $p$ - $i$ - $n$  diodes were achieved through the enhancement of the hole-initiated multiplication.

The authors acknowledge the Fulbright Association and the Spanish Ministry of Education and Science for supporting one of the authors (J.L.P.).

- <sup>1</sup>A. L. Beck, B. Yang, X. Guo, and J. C. Campbell, *IEEE J. Quantum Electron.* **40**, 321 (2004).
- <sup>2</sup>J. B. Limb, D. Yoo, J. H. Ryou, W. Lee, S. C. Shen, R. D. Dupuis, M. L. Reed, C. J. Collins, M. Wraback, D. Hanser, E. Preble, N. M. Williams, and K. Evans, *Appl. Phys. Lett.* **89**, 011112 (2006).
- <sup>3</sup>K. A. McIntosh, R. J. Molnar, L. J. Mahoney, K. M. Molvar, N. Efremow, Jr., and S. Verghese, *Appl. Phys. Lett.* **76**, 3938 (2000).
- <sup>4</sup>R. McClintock, J. L. Pau, K. Minder, C. Bayram, P. Kung, and M. Razeghi, *Appl. Phys. Lett.* **90**, 141112 (2007).
- <sup>5</sup>K. Minder, J. L. Pau, R. McClintock, P. Kung, C. Bayram, M. Razeghi, and D. Silversmith, *Appl. Phys. Lett.* **91**, 073513 (2007).
- <sup>6</sup>J. L. Pau, R. McClintock, K. Minder, C. Bayram, P. Kung, M. Razeghi, E. Muñoz, and D. Silversmith, *Appl. Phys. Lett.* **91**, 041104 (2007).
- <sup>7</sup>X. Guo, L. B. Rowland, G. T. Dunne, J. A. Fronheiser, P. M. Sandvik, A. L. Beck, and J. C. Campbell, *IEEE Photonics Technol. Lett.* **18**, 136 (2006).
- <sup>8</sup>J. C. Campbell, A. G. Dentai, W. S. Holden, and B. L. Kasper, *Electron. Lett.* **19**, 818 (1983).
- <sup>9</sup>S. Pellegrini, R. E. Warburton, L. J. J. Tan, J. S. Ng, A. B. Krysa, K. Groom, J. P. R. David, S. Cova, M. J. Robertson, and G. S. Buller, *IEEE J. Quantum Electron.* **42**, 397 (2006).
- <sup>10</sup>J. C. Carrano, D. J. H. Lambert, C. J. Eiting, C. J. Collins, T. Li, S. Wang, B. Yang, A. L. Beck, R. D. Dupuis, and J. C. Campbell, *Appl. Phys. Lett.* **76**, 924 (2000).
- <sup>11</sup>K. A. McIntosh, R. J. Molnar, L. H. Mahoney, A. Lightfoot, M. W. Geis, K. M. Molvar, I. MeIngailis, R. L. Aggarwal, W. D. Woodhue, S. S. Choi, D. L. Spears, and S. Verghese, *Appl. Phys. Lett.* **75**, 3485 (1999).